AIAA JOURNAL
Vol. 37, No. 11, November 1999

Structural Optimization with Static Aeroelastic and Stress Constraints Using Expandable Modal Basis

M. Karpel* and B. Moulin†
Technion—Israel Institute of Technology, 32000 Haifa, Israel
and
M. H. Love‡
Lockheed Martin Tactical Aircraft Systems, Fort Worth, Texas 76101

Recent developments of the modal-based aeroelastic optimization approach facilitated efficient treatment of static-aeroelastic and stress constraints. The reduced-size models use low-frequency normal modes of the baseline structure as fixed generalized coordinates throughout the optimization process. The modal approach is extended to allow the expansion of the modal basis by the addition of static modes generated in previous design steps. Being based on modal perturbations stored in the modal data base before the optimization process starts, the basis expansion accelerates the convergences to the optimal design. Numerical examples with realistic fighter-aircraft models demonstrate practical applications with CPU speed-up factors of ~10, compared with the regular discrete-coordinate approach, with negligible loss of accuracy.

Introduction

THE desire for efficient procedures for optimal design of complex structures motivated the development of reduced-size optimization schemes in which calculations of stability and response parameters and their sensitivity to changes in the design variables are based on a set of low-frequency vibration modes of a baseline structure. The modal approach is especially attractive in multidisciplinary cases in which the excitation loads are affected by the structural response, such as in aeroelastic and control-augmented systems.

The ASTROS code[1] was developed to provide a multidisciplinary analysis and design capability for aerospace structures. The considered disciplines include structural analysis, aeroelastic analysis, and some features of the interaction with the control system. As in other commonly used analysis and optimization schemes,[2–4] the dynamic response and the stability features are treated by the modal approach, but the static-aeroelastic and stress disciplines are treated by the discrete approach.

The use of modal coordinates in static-aeroelastic analysis was shown in Ref. 5 to be extremely efficient and of good accuracy in application to realistic aircraft models. Structural optimization with static-aeroelastic constraints was later performed with the baseline normal modes serving as a fixed set of generalized coordinates throughout the entire optimization run.[6] The fixed-modal-basis approach was shown in Ref. 6 to be of good accuracy with design variable changes of less than ~20%. Larger changes required the update of the full finite-element model such that the optimization process could be resumed with new modal coordinates. Even when the modal approach was successfully applied in multidisciplinary optimization with static- and dynamic-aeroelastic constraints,[7] it was not ready yet for application to stress constraints.

The main reason for not using the modal approach for stresses was that it might yield erroneous results in cases of concentrated loads and in cases of local structural changes. Recent developments of the modal approach facilitated the application of practical techniques to overcome these difficulties with minimal impact on the computational efficiency. Fictitious masses,[8] which are added to the structure when the baseline modal coordinates are defined, can be used to deal with local excitation. High-accuracy stresses can be obtained in modal-based structural optimization by use of modal perturbations.[9] The application of the modal approach[10] in ASTROS was most effective in the aeroelastic effectiveness and trim part, with speed-up factors of ~80 and an error level of less than 1%. The application of the modal approach for stress constraints showed speed-up factors of ~4 with error levels of 10%. The cost effectiveness of the modal approach in dealing with stress constraints was improved in Ref. 11 when the decomposed stiffness matrix of the baseline structure was used to produce high-order approximations of the deformations that were due to local stiffness changes.

The formulations in Refs. 9–11 used a fixed generalized coordinate basis (the normal modes of the baseline structure) throughout the optimization, with the displacement vector for stress analysis of each design case reevaluated in every design iteration. Being affected by the modal perturbations mentioned above, these displacement vectors contain important information that is not contained in the normal modes. In Refs. 12 and 13 static displacement modes were used as reduced-basis generalized coordinates for reanalysis of truss structures under fixed loads. The method described in this paper uses static modes that are based on the displacement vectors for stress analysis calculated during the optimization process. The static modes of one design step (iteration) are used to expand the modal basis of the next step in a way that accommodates changes in the external loads that are due to aeroelastic effects. The expanded reduced-basis model is applied in structural optimization with static-aeroelastic and stress constraints.

Aeroelastic Equilibrium in Modal Coordinates

The equilibrium equation for discrete-coordinate static analysis of a free–free structure is

$$[K_{aa}]\{u_a\} + [M_{aa}]\{\ddot{u}_a\} = \{P_a\} \tag{1}$$

where $[K_{aa}]$ and $[M_{aa}]$ are stiffness and mass matrices, $\{u_a\}$ is the displacement vector, and $\{P_a\}$ is the external-load vector that depends on $\{u_a\}$ and on the rigid-body velocities that are due to aeroelastic effects. The accelerations $\{\ddot{u}_a\}$ are assumed to be due to rigid-body acceleration only. The discrete analysis coordinates in which Eq. (1) is expressed are called a-set coordinates. These are the coordinates remaining after the elimination of those that depend on others, those constrained by boundary conditions, and

Presented as Paper 98-1868 at the AIAA/ASME/ASCE/AHS/ASC 39th Structures, Structural Dynamics, and Materials Conference, Long Beach, CA, 20–23 April 1998; received 26 August 1998; revision received 19 February 1999; accepted for publication 12 June 1999.

*Professor, Faculty of Aerospace Engineering. Senior Member AIAA.
†Research Associate, Faculty of Aerospace Engineering.
‡Engineering Specialist Senior, Technology Integration. Senior Member AIAA.

those reduced by static condensation. For the sake of simplicity, the discrete-coordinate equations in this paper are expressed at the a-set level, even though some computations are actually performed at higher-level sets of coordinates. A detailed description of the various coordinate sets and the transformations between them in modal-based analysis is given in Refs. 11 and 14.

The basic assumption of the modal approach is that the structural displacements during response to external excitation can be adequately expressed as a linear combination of the rigid-body modes $[\phi_{ar}]$ and a set of low-frequency normal modes $[\phi_{ae}]$ of the baseline structure:

$$\{u_a\} = [\phi_{ar}]\{\xi_r\} + [\phi_{ae}]\{\xi_e\} \tag{2}$$

where $\{\xi_r\}$ and $\{\xi_e\}$ are the vectors of rigid-body and elastic modal displacements, respectively. The substitution of Eq. (2) into Eq. (1) and the premultiplication by $[\phi_{ar}\ \phi_{ae}]^T$ while neglecting the effects of $\{\ddot{\xi}_e\}$ yields

$$\begin{bmatrix} 0 \\ K_{ee} \end{bmatrix}\{\xi_e\} + \begin{bmatrix} M_{rr} \\ M_{er} \end{bmatrix}\{\ddot{\xi}_r\} = \begin{bmatrix} \phi_{ar}^T \\ \phi_{ae}^T \end{bmatrix}\{P_a\} \tag{3}$$

which is applied throughout the optimization process with the same set of baseline modes. For the baseline structure, $[K_{ee}]$ is diagonal and $[M_{er}] = 0$, but not for the modified structure. The derivatives of $[K_{ee}]$, $[M_{rr}]$, and $[M_{er}]$ with respect to the design variables are stored in the database before the optimization starts and are used to update the generalized matrices during the optimization process. The processes of updating the generalized matrices and recalculating the modal deformations and the associated aerodynamic loads are detailed in Refs. 10 and 11.

Linear static-aeroelastic codes are commonly based on aerodynamic panel methods that produce Mach-dependent force coefficient matrices that relate aerodynamic loads on the panels to local angles of attack. Premultiplications and postmultiplications of the panel matrices by modal deflections and slopes, transformed to the aerodynamic grid by spline techniques, generate the generalized steady aerodynamic force coefficient matrices $[A_{rr}]$, $[A_{re}]$, $[A_{er}]$, and $[A_{ee}]$ associated with the rigid-body and the elastic modal displacements. The splined modes can also be used to generate the generalized force coefficient matrices $[A_{r\delta}]$ and $[A_{e\delta}]$, where the subscript δ relates to the vector $\{\delta\}$ of trim variables such as angle of attack, control surface deflection, and roll rate.

The formulation and solution of static-aeroelastic equilibrium equations in modal coordinates were presented in Refs. 10 and 11. A general form of the equilibrium equation is

$$\begin{bmatrix} -qA_{rr} & -qA_{re} & M_{rr} \\ -qA_{er} & K_{ee} - qA_{ee} & M_{er} \\ M_{rr} & M_{er}^T & 0 \end{bmatrix}\begin{Bmatrix} \xi_r \\ \xi_e \\ \ddot{\xi}_r \end{Bmatrix} = \begin{bmatrix} qA_{r\delta} \\ qA_{e\delta} \\ 0 \end{bmatrix}\{\delta\} \tag{4}$$

where q is the dynamic pressure. The last row in Eq. (4) relates rigid-body displacements to the elastic ones. For the baseline structure $[M_{er}] = 0$ and hence $\{\xi_r\} = 0$. However, when the structure changes, a nonzero $\{\xi_r\}$ is needed to enforce orthogonality between the elastic deformations and the rigid-body modes. The elimination of $\{\xi_r\}$ and $\{\xi_e\}$ from Eq. (4) yields the trim equation[10]

$$[M_{rr}]\{\ddot{\xi}_r\} = q[\tilde{A}_{r\delta}]\{\delta\} \tag{5}$$

The flex-to-rigid ratios between terms in $[\tilde{A}_{r\delta}]$ of Eq. (4) and $[A_{r\delta}]$ of Eq. (5) define the aeroelastic effectiveness parameters that can be used as optimization constraints. The solution of Eq. (5) for the n_r free trim variables (where n_r is the number of rigid-body modes) and the recovery of $\{\xi_r\}$ and $\{\xi_e\}$ by Eq. (4) facilitates the calculation of the net loads:

$$\{P_a\} = [P_1]\{\delta\} + [P_2]\{\xi_r\} + [P_3]\{\xi_e\} - [M_{aa}][\phi_{ar}]\{\ddot{\xi}_r\} \tag{6}$$

where $[P_1]$, $[P_2]$, and $[P_3]$ are aerodynamic load matrices that are due to trim parameters and modal displacements.

It can be observed that the trim variables, net loads, and effectiveness constraints are functions of the design variables. The differentiation of Eqs. (4–6) with respect to the design variables results in analytical sensitivity expressions.[10] The order of Eq. (4) is typically 2 to 3 orders of magnitude smaller than the equivalent one in common discrete-coordinate schemes, which facilitates huge computation time savings in modal-based optimization with static-aeroelastic considerations. The accuracy of the modal approach has been shown to be very high in several realistic static-aeroelastic design studies.[6,9–11]

Stress/Strain Analysis

Element stresses and strains can be related to the structural displacements by

$$\{\sigma\} = [SU]\{u_l\} \tag{7}$$

where $[SU]$ is a fixed matrix and $\{u_l\}$ is a subset of $\{u_a\}$ obtained after n_r selected degrees of freedom are clamped to eliminate rigid-body displacements. One can calculate the displacement vector by the basic modal assumption of Eq. (2), but the adequacy of the substitution of the resulting $\{u_l\}$ in Eq. (7) for calculating stresses is questionable. References 9–11 showed that, with a fair number of elastic modes (typically 20–50) taken into account, the modal assumption that uses the baseline modes as fixed generalized coordinates is adequate for stress/strain analysis only when it is applied to the baseline structure. When applied to a modified structure, baseline modes might yield grossly inaccurate stresses and strains. Hence the fixed-basis modal approach needed to be modified in order to be applied with stress and strain considerations.

Once the the modal-based aeroelastic trim analysis is performed, the most accurate way to perform stress/strain analysis is by updating the full finite-element stiffness matrix and solving for displacements under the updated loads of Eq. (6). This hybrid approach is easy to implement when the modal and discrete schemes are integrated in one code.[11] It is typically much less inefficient, however, than the modal-based alternatives discussed next.

Reference 9 modified the basic modal approach by supplementing the modal database with modal perturbations calculated before the optimization starts. A first-order approximation of the displacement vector for stress analysis of the modified structure was expressed as

$$\{u_l\} = \{u_l\}_b + \{\Delta u_l^{(1)}\} \tag{8}$$

where $\{u_l\}_b$ is the elastic displacement of the baseline structure under the modified net loads and $\{\Delta u_l^{(1)}\}$ is the incremental displacement change that is due to forces applied by the added material on the baseline structure. The first term of Eq. (8) can be formulated by the mode-displacement (MD) approach as[9]

$$\{u_l\}_{b_{\mathrm{MD}}} = [\phi_{le}]\left([I] + [K_{ee}]_b^{-1}\left[\sum_{i=1}^{n_{dv}}(v_i - v_{b_i})[K_{ee}]_i\right]\right)\{\xi_e\} \tag{9}$$

where $[I]$ is a unit matrix, $[K_{ee}]_b$ is the generalized stiffness matrix of the baseline structure, and $[K_{ee}]_i$ is its derivative with respect to the ith design variable v_i. Alternatively, when the discrete and the modal-based codes are integrated, it is more effective to use the summation-of-force (SOF) approach with the already decomposed baseline stiffness matrix $[K_{ll}]_b$ to calculate

$$\{u_l\}_{b_{\mathrm{SOF}}} = [K_{ll}]_b^{-1}\{P_l\} \tag{10}$$

where $\{P_l\}$ is the l-set partition of $\{P_a\}$ of Eq. (6). Comparisons between the use of the MD and the SOF approaches in modal-based optimization are given in Refs. 11 and 14.

The second term in Eq. (8) is

$$\{\Delta u_l^{(1)}\} = [K_{ll}]_b^{-1}\left[\sum_{i=1}^{n_{dv}}(v_i - v_{b_i})[\phi_{\mathrm{Fl}}]_i\right]\{\xi_e\} \tag{11}$$

where

$$[\phi_{\mathrm{Fl}}]_i = -\frac{\partial[K_{ll}]}{\partial v_i}[\phi_{le}]$$

is a modal force perturbation matrix associated with the ith design variable. The perturbation matrices are stored in the database before the optimization starts.[10] Analytical expressions for the sensitivity

of stress and strain constraints in design maneuver load cases, which take into account load redistribution effects, are given in Refs. 9–11. Reference 11 used the first-order displacement approximation of Eq. (8) to calculate higher-order approximations in an iterative process.

A detailed comparison between the alternative schemes of Refs. 10 and 11 for solving large aeroelastic optimization problems is given in Ref. 11. A good tradeoff between efficiency and accuracy for typical design optimization problems with several thousands degrees of freedom was the first-order SOF alternative. Higher-order approximations improved the accuracy of the analyzed stresses, but somewhat slowed down the modal-based process. It is shown in the following sections that, in an optimization process based on several design steps, it is more effective to use the first-order displacement vector of Eq. (8), as calculated at one design step, for defining a generalized coordinate that expands the modal basis in the following step.

Expanded Modal Matrices

Static modes can be added to the modal basis after the baseline analysis and the first design iteration are completed. The starting point in defining an additional mode is the incremental displacement change of Eq. (11), as calculated in the first design iteration, which can be expressed as

$$\{\bar{\phi}_{ls}\} = [K_{ll}]_b^{-1}\{\bar{P}_l\} \tag{12}$$

where

$$\{\bar{P}_l\} = \left[\sum_{i=1}^{n_{dv}} (v_i - v_{b_i})[\phi_{Fl}]_i\right]\{\bar{\xi}_e\}$$

where $\{\bar{\xi}_e\}$ is the vector of generalized elastic deflections in the preceding iteration.

The deflection vector $\{\bar{\phi}_{ls}\}$ is orthogonalized with respect to baseline modes $[\phi_{le}]$ by

$$\{\phi_{ls}\} = \{\bar{\phi}_{ls}\} - [\phi_{le}][K_{ee}]_b^{-1}[\phi_{le}]^T\{\bar{P}_l\} \tag{13}$$

which can be shown, with Eqs. (1–3) and (12), to be orthogonal to the existing modal coordinates with respect to the baseline stiffness matrix, namely,

$$[\phi_{le}]^T[K_{ll}]_b\{\phi_{ls}\} = \{0\} \tag{14}$$

The first static mode is added in the second iteration, with Eq. (12) calculated with the original database matrices and the n_e modal deflections of the first iteration. The database matrices are then expanded such that the analysis and the sensitivity of the modified structures can be performed as described in Ref. 11, but with the expanded basis of $n_z = n_e + 1$ modes. The baseline-mode matrix is expanded by

$$[\phi_{lz}] = [\phi_{le} \quad \phi_{ls}] \tag{15}$$

The baseline generalized stiffness matrix becomes

$$[K_{zz}]_b = \begin{bmatrix} K_{ee_b} & 0 \\ 0 & K_{ss} \end{bmatrix} \tag{16}$$

where, as implied by Eqs. (12–14), the added diagonal term is

$$K_{ss} = \{\phi_{ls}\}^T[K_{ll}]_b\{\phi_{ls}\} = \{\phi_{ls}\}^T\{\bar{P}_l\} \tag{17}$$

The baseline $[M_{er}]$ in Eq. (3) is expanded by

$$[M_{zr}]_b = \begin{bmatrix} 0 \\ \{\phi_{as}\}^T[M_{aa}]_b[\phi_{ar}] \end{bmatrix} \tag{18}$$

where $\{\phi_{as}\}$ is the merge of $\{\phi_{ls}\}$ and zeros at the n_r clamped coordinates discussed after Eq. (7).

Subsequent iterations are performed with the expanded database matrices. New static modes are calculated at the end of each iteration. These modes affect the modal-based model in one of three ways:

1) If the number of already added modes n_s is equal to a maximum number $n_{s_{max}}$ specified by the user, the new mode is orthogonalized with respect to the first $n_e + n_s - 1$ modes and then simply replaces the last added mode.

2) If $n_s < n_{s_{max}}$, the new mode is orthogonalized with respect to all the existing $n_e + n_s$ modes and its K_{ss_j} value is calculated. If $K_{ss_j} > K_{ee_1} \times 10^{-6}$ (of the first elastic mode), the mode is added to the generalized coordinates as described above (with the already added static modes treated as normal modes).

3) If $K_{ss_j} \le K_{ee_1} \times 10^{-6}$, the new mode is not added to avoid singularity of the expanded $[K_{zz}]_b$.

The aerodynamic force coefficients associated with the added modes are used to expand the generalized aeromatrices in the static-aeroelastic trim and loads equations. In this way, the added modes improve also the accuracy of the aeroelastic trim and effectiveness solutions along the optimization path, which were not affected by the model perturbations of the preceding section.

Numerical Examples

Two sample design optimization applications are described in this section, one performed at Technion during the development of the modal-based ASTROS module, and one performed at Lockheed Martin Tactical Aircraft System in an investigation of aircraft design sensitivity to aeroelastic roll efficiency. The two applications were performed with similar wing-tailed fighter-aircraft models, but with different wings, and with identical load conditions and design constraints.

The Technion numerical example is based on a generic advanced fighter composite-wing (AFC) ASTROS model with an all-movable horizontal tail and four control surfaces on each wing, in which only the two trailing-edge ones used for maneuvering. The aerodynamic panel model of Carmichael et al.[15] is shown in Fig. 1. The associated aerodynamic force coefficient matrix was imported from another code. The structural model consists of 1276 grid points and 4449 elements and has 3762 free degrees of freedom with symmetric boundary conditions and 3797 with antisymmetric ones. A top view of the wing structural model, in which the wing box is divided into 13 zones, is shown in Fig. 2. The thicknesses of the 0-, ±45-, and 90-deg direction plies in the upper and the lower skins are used as design variables (for a total of 78 design variables). The structural arrangement and the design zones are identical to those used in Refs. 10, 11, and 14, except that the wing skin there was made of aluminum.

The wing box is optimized for minimum weight under the strain, aileron effectiveness, and roll-rate constraints specified in Table 1. Modal-based optimization runs were performed with 48 symmetric elastic modes and 49 antisymmetric ones. Results for modal runs with various strain analysis options, with and without static modes added to the modal basis, are compared below with results obtained by a standard discrete-coordinate ASTROS run. Optimization histories for the reference discrete optimization case and for various modal-based options without static modes added are compared in Fig. 3. It can be observed that, even when the modal basis is not expanded, the overall accuracy of the modal-based optimization is quite good, even though the weight of the changeable elements is reduced by a total of 30%. The total weight errors with the first-order

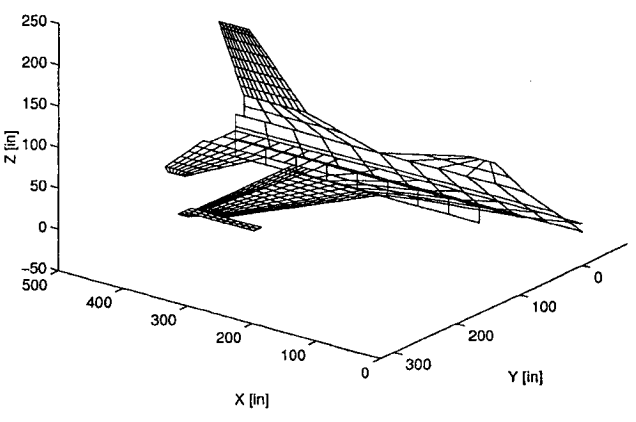

Fig. 1 Aerodynamic AFC panel model.

Table 1 Design loads and constraints

Load condition	Design constraint
Mach 0.95, 10,000 ft, 9-g pullup	Fiber strain: 3000-$\mu\epsilon$ tension, 2800-$\mu\epsilon$ compression
Mach 1.20, sea level, −3-g pushover	Fiber strain: 3000-$\mu\epsilon$ tension, 2800-$\mu\epsilon$ compression
Mach 0.95, 10,000 ft, maximum steady roll	Aileron effectiveness ≥ 0.2373
Mach 1.20, sea level, maximum steady roll	Roll-rate constraint

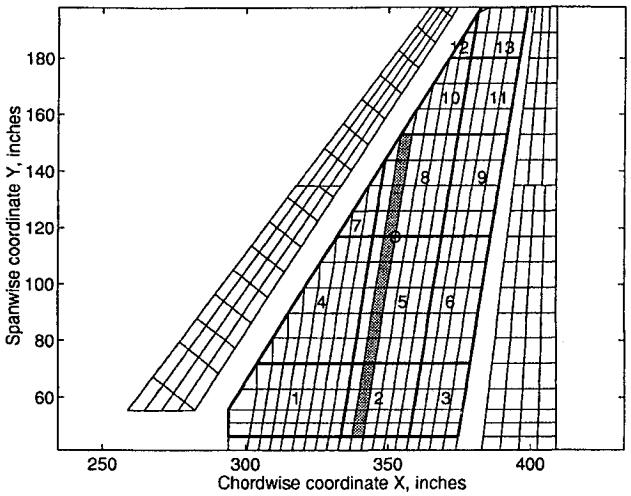

Fig. 2 AFC wing structural model.

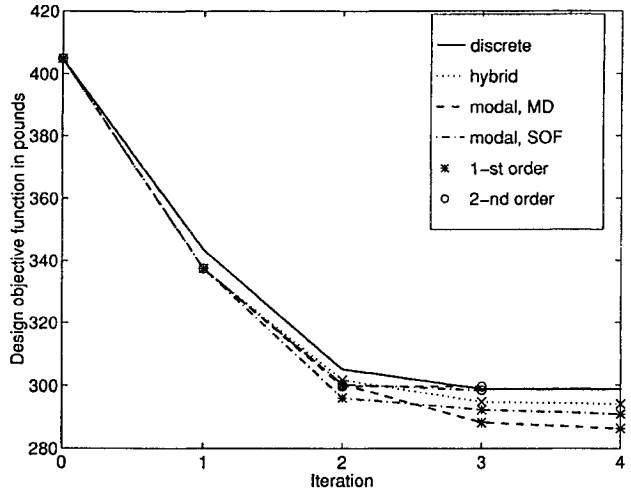

Fig. 3 Optimization weight history without static modes.

approximations were 2–4%, whereas those of the hybrid and the second-order methods were 0–1%. The same optimization cases, but with a single static mode added to the modal basis, are shown in Fig. 4. Now all the fully modal cases are within 1% of the discrete case, and the hybrid case converges to the discrete one exactly in spite of the slight error after the first design step.

The errors in calculating the skin principal strains in the second iteration of the modal cases of Fig. 4 were established by comparison of the modal strains with those of the discrete case. The rms strain errors are shown in Fig. 5 in percentage of the maximum allowable strain in tension. The CPU time per design iteration in the various options, not including the setup time for constructing the database, are given in Table 2. The setup CPU time for constructing the database was 578 s. The CPU time for running the discrete case was 311 s in the preface stage and then 501 s per iteration. The SOF modal case with one static mode is probably the most cost-effective option in typical design studies. In our study it reduced the CPU time

Table 2 CPU seconds for design iterations with modal methods

	Static mode	
Method	No	One
Hybrid		
First design iteration	34.0	34.0
Other iterations	107.0	153.0
SOF		
First design iteration	38.5	38.5
Other, first order	62.7	90.9
Other, second order	176.6	204.8
MD		
First design iteration	31.5	31.5
Other, first order	56.9	86.0
Other, second order	175.7	203.9

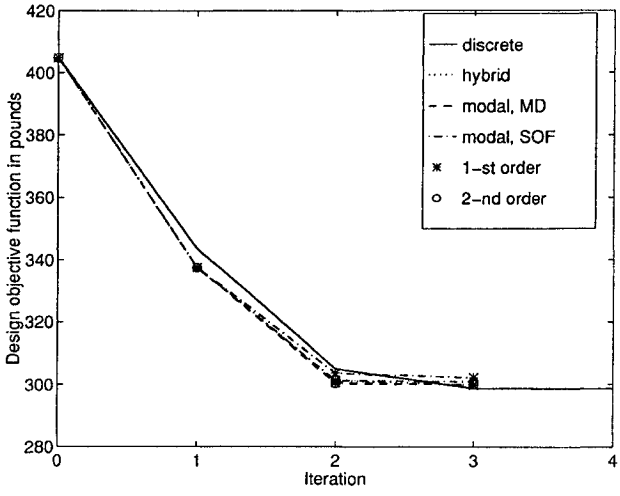

Fig. 4 Optimization weight history with one static mode.

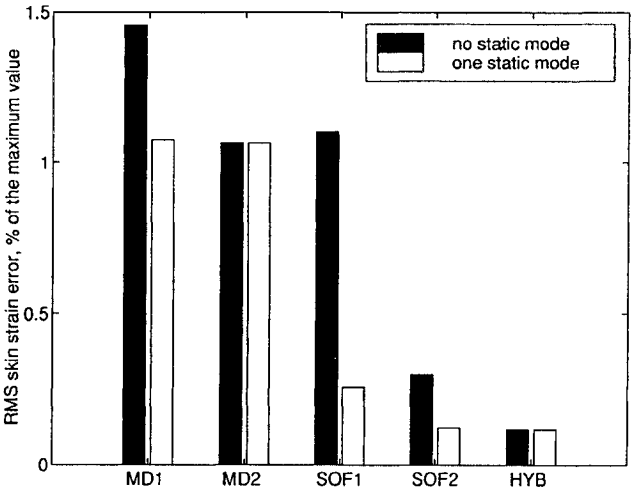

Fig. 5 Root-mean-square skin principal strains errors.

per iteration by 82% compared with that of to the discrete case, with rms skin strain errors of 0.2%. The setup time for constructing the modal database is not very important because the same database can be used for numerous optimization cases with various move limits, constraints, and control gearing ratios.

The Lockheed Martin verification of the modal-based optimization method was done by using it in a typical fighter roll effectiveness trade study. To verify the applicability of the modal-based approach, an application should provide identical results for both the discrete and the modal-based methods. A case study was selected from an aeroelastic tailoring study previously presented by Barker and Love.[16] The design study involved the development of structural

design sensitivity to roll efficiency for a typical fighter. Two different aeroelastic tailoring concepts were found to satisfy the roll effectiveness and the minimum weight requirements. Weisshaar and Nam[17] discovered a similar phenomenon in their study concerning simultaneous optimization of aileron location and aeroelastic tailoring. The design space contains two optima, and design optimization results are very sensitive to the starting point and design sensitivity accuracy. Consequently this case provides a challenge for the modal-based approach to reproduce this design.

The ASTROS model of the typical wing-tailed fighter used in this study is described in Ref. 16. The vehicle model is similar to that shown in Fig. 1, except that the wing here is with a 10% smaller aspect ratio and has only two control surfaces per wing, a flaperon (inboard flap/aileron) and a leading-edge flap. The aircraft trims in pitch conditions with the horizontal tails. In roll conditions, the aircraft trims with the flaperons at subsonic conditions and with the flaperons and horizontal tails at supersonic conditions. The vehicle is depicted for this study through a steady aerodynamic panel model, a structural finite-element model, and a design model.

A flat linear panel model representing the basic planform geometry of the fighter aircraft was used. A total of 395 aerodynamic panels were used: 252 horizontal panels and 143 vertical panels. Aerodynamic results were produced at Mach 0.95 and Mach 1.20 for both symmetric and antisymmetric conditions. Although use of linear theory aerodynamics in the transonic regime is undesirable, it was in general practice in preliminary design at the time of the original study.

The structural model represents a preliminary design finite-element model of the fighter aircraft. The wing model is more elaborate than the one shown in Fig. 2. The model consists of a dynamics-oriented fuselage/empennage and a stress-oriented wing. This model is adequate for basic wing skin sizing, development of internal loads for sizing of wing component parts, and determination of wing-to-fuselage carry-through load distribution for sizing in fuselage structure. A composite wing skin is modeled to allow aeroelastic and reduced-weight performance studies. Specifically, the composite wing skins are designed in thickness and percentage of thickness to orientations for specified roll rate and structural integrity at maneuver conditions.

The physical design variable arrangement represents the design variables for a single composite layer (i.e., 0-, ±45-, or 90-deg layer). In this fashion, each layer for both upper and lower skins was designed distinctly. The ply directions, however, remain fixed, with the 0-deg plies oriented at 27-deg sweep aft (nearly parallel to the box leading-edge spar). The physical variables were formulated with the ELIST data entry of ASTROS to arrive at a total of 174 design variables. A baseline aluminum skin model was also designed to provide reference to improvements in weight and roll performance that were due to aeroelastic tailoring.

The composite skin trade study designs consisted of the four load conditions and corresponding design constraints listed in Table 1. The design trade of Ref. 16 evaluated the optimum wing skin weight as a function of maximum steady-state roll rate for a Mach 1.20, sea-level, flight condition. Design points were selected as a function of percent increase over the baseline aluminum design roll rate. Four roll-rate constraints were evaluated: 0, 25, 35, and 45% over the baseline value. The strain allowables were derived as far-field damage tolerance allowable strain in the fiber direction. Such values are based on delamination growth after low-velocity impact. The aileron effectiveness constraint is the value obtained for the aluminum skin model.

In the case of testing the capability of the modal approach to acquire the same design as that of a discrete approach, the design that achieved a 35% improvement in roll effectiveness and the lowest weight as shown Ref. 16 was selected. The setup of the modal run included 50 modes in the symmetric boundary condition and 63 modes in the antisymmetric boundary condition. The first-order SOF approach along with one static mode was used for approximation in the analysis and sensitivities. As shown by the weight iteration history of Fig. 6, both designs converged to the same weight. The discrete approach required over 600 min of CPU time, whereas the modal approach required less than 45 min of CPU time on the same workstation. However, the proof of whether the modal approach captured the discrete design is in the examination of the behavior of the design and the composite material definition.

Table 3 Design comparisons of aeroelastic behavior

Maneuver condition		Rigid coefficient	Flexible coefficient: Discrete	Flexible coefficient: Modal
Mach 0.95, 10,000 ft, symmetric	$C_{L\alpha}$	0.091	0.0867	0.0867
	$C_{M\alpha}$	−0.0092	−0.0076	−0.0080
Mach 1.20, sea level, symmetric	$C_{L\alpha}$	0.0970	0.0878	0.0855
	$C_{M\alpha}$	−0.0280	−0.0174	−0.0186
Mach 0.95, 10,000 ft, antisymmetric	$C_{l\delta}$	0.0037	0.0018	0.0018
	C_{lp}	−0.0077	−0.0070	−0.0073
Mach 1.20, sea level, antisymmetric	$C_{l\delta}$	0.0013	−0.0001	−0.0001
	C_{lp}	−0.0087	−0.0086	−0.0086

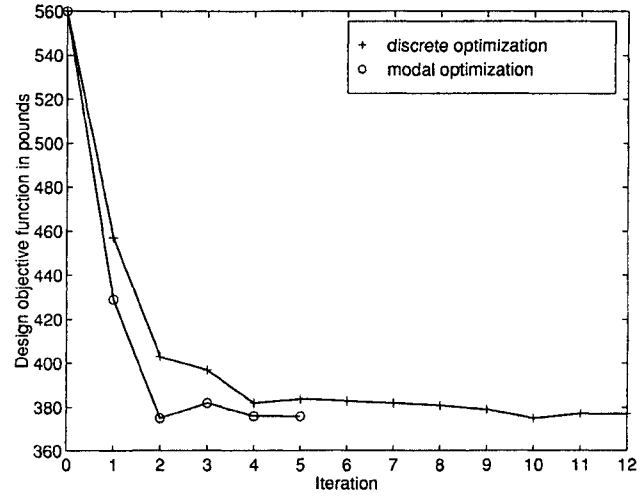

Fig. 6 Typical optimization weight history in the roll effectiveness trade study.

Table 3 shows the aeroelastic behavior of the designs for the maneuver conditions used in the design optimization. The table exhibits stability coefficient data for the rigid aerodynamic model, the discrete design optimization, and the modal design optimization. The modal and the discrete designs are similar in their static-aeroelastic performance. The largest differences occur in $C_{L\alpha}$ and $C_{M\alpha}$ for the supersonic case and C_{lp} for the subsonic case. It can be observed that the rolling coefficient that is due to flaperon rotation $C_l\delta$ at Mach 1.2 is reversed, which explains the need for horizontal tail participation in the rolling maneuver.

Figures 7 and 8 provide highlights of the modal and the discrete composite designs. In a design with directional composite materials, there is a combinatorial number of ways to achieve similar aeroelastic tailoring goals. For the modal method to be substantiated, it is imperative to be able to achieve consistent design concepts to the discrete approach. As indicated in these figures, the modal method achieved the same design as the discrete approach. Shown in Fig. 7 are the discrete design thicknesses of the upper skin orientations of balanced ±45 deg. Figure 8 contains the difference from the discrete design to the modal design. There are small differences, particularly in the areas where the composite wing skin is thin to begin with and the deformations are small to begin with (i.e., the wing tip). These comparisons are indicative of the other comparisons in wing skin thickness.

Future studies with the modal approach include exploiting its efficiency in a design of experimental roles to consider development of data for response surfaces. Such areas as interactions with controls, manufacturing, and material variability can be studied within accuracy of the finite-element domain without the costs of large finite element models.

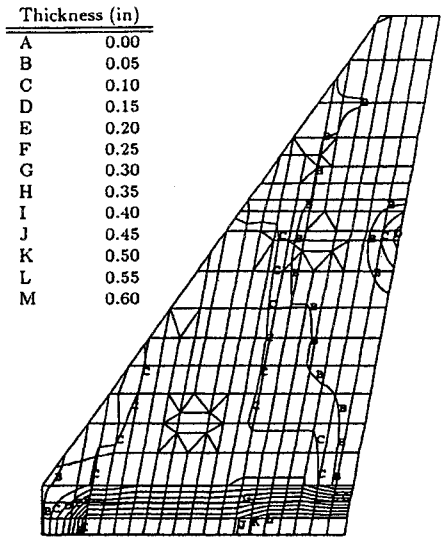

Fig. 7 Wing box skin thickness contour: discrete design.

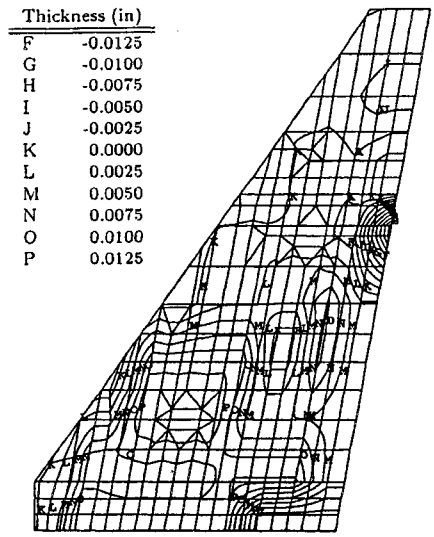

Fig. 8 Wing box skin thickness contour: modal minus discrete designs.

Conclusions

The modal-based structural optimization method was extended to allow the expansion of the modal database with static modes calculated during the design process. The expanded basis improves the accuracy of the modal approach and yields asymptotic convergence to the exact discrete-coordinate design. The improvements enhance the performance of the modal-based ASTROS module as an on-line multidisciplinary design tool. The composite wing case studies were with relatively large number of design variables (78 and 174). They were indicative that the modal approach to aeroelastic design has great potential in the preliminary design of aircraft for which answers to what-if-type questions are needed in short order. The modal approach is accurate to produce results quite similar to those of the discrete approach, not only in terms of system behavior but also in consistent design concepts.

Acknowledgments

The work of M. Karpel and B. Moulin was conducted under contract with Lockheed Martin Tactical Aircraft Systems. The work of M. H. Love was partially supported by the Israeli Ministry of Immigrant Absorption. Technical support of V. B. Venkayya and the Wright Laboratory/Flight Dynamics Directorate is gratefully acknowledged.

References

[1]Neill, D. J., Johnson, E. H., and Canfield, R. A., "ASTROS—A Multidisciplinary Automated Structural Design Tool," *Journal of Aircraft*, Vol. 27, No. 12, 1990, pp. 1021–1027.

[2]Climent, H., and Johnson, E. H., "Aeroelastic Optimization Using MSC/NASTRAN," *Proceedings of the International Forum on Aeroelasticity and Structural Dynamics*, Association Aéronautique et Astronautique de France, Paris, 1993, pp. 1097–1116.

[3]Livne, E., Schmit, L. A., and Friedmann, P. P., "Integrated Structure/Control/Aerodynamic Synthesis of Actively Controlled Composite Wings," *Journal of Aircraft*, Vol. 30, No. 3, 1993, pp. 387–394.

[4]Bindolino, G., Lanz, M., Mantegazza, P., and Ricci, S., "Integrated Structural Optimization in the Preliminary Aircraft Design," *Proceedings of the 17th Congress of the International Council of the Aeronautical Sciences*, International Council of the Aeronautical Sciences, Amsterdam, 1990, pp. 1366–1378.

[5]Sheena, Z., and Karpel, M., "Static Aeroelastic Analysis Using Aircraft Vibration Modes," *Collected Papers of the Second International Symposium on Aeroelasticity and Structural Dynamics*, DGLR, Bonn, 1985, pp. 229–232.

[6]Karpel, M., and Sheena, Z., "Structural Optimization for Aeroelastic Control Effectiveness," *Journal of Aircraft*, Vol. 26, No. 8, 1989 pp. 493–495.

[7]Karpel, M., "Multidisciplinary Optimization of Aeroservoelastic Systems Using Reduced-Size Models," *Journal of Aircraft*, Vol. 29, No. 5, 1992, pp. 939–946.

[8]Karpel, M., and Presente, E., "Structural Dynamic Loads in Response to Impulsive Excitation," *Journal of Aircraft*, Vol. 32, No. 4, 1995, pp. 853–861.

[9]Karpel, M., and Brainin, L., "Stress Considerations in Reduced-Size Aeroelastic Optimization," *AIAA Journal*, Vol. 33, No. 4, 1995, pp. 726–722.

[10]Karpel, M., Moulin, B., and Love, M. H., "Modal-Based Structural Optimization with Static Aeroelastic and Stress Constraints," *Journal of Aircraft*, Vol. 34, No. 3, 1997, pp. 433–440.

[11]Karpel, M., "Modal-Based Enhancement of Integrated Structural Design Optimization Schemes," *Journal of Aircraft*, Vol. 35, No. 3, 1998, pp. 437–444.

[12]Kirsch, U., "Reduced Basis Approximations of Structural Displacements for Optimal Design," *AIAA Journal*, Vol. 29, No. 10, 1991, pp. 1751–1758.

[13]Kirsch, U., "Improved Stiffness-Based First-Order Approximations for Structural Optimization," *AIAA Journal*, Vol. 33, No. 1, 1995, pp. 143–150.

[14]Moulin, B., and Karpel, M., "Static Condensation in Modal-Based Structural Optimization," *Structural Optimization*, 1998, Vol. 15, No. 3/4, pp. 275–283.

[15]Carmichael, R. L., Castellano, C. R., and Chen, C. F., "The Use of Finite Element Method for Predicting the Aerodynamics of Wing-Body Combinations," *Analytic Methods in Aircraft Aerodynamics*, NASA SP-228, 1970, pp. 37–51.

[16]Barker, D. K., and Love, M. H., "An ASTROS Application with Path Dependent Results," *Proceedings of the AIAA 6th Multidisciplinary Analysis and Optimization Conference*, AIAA, Reston, VA, 1996, pp. 1334–1343.

[17]Weisshaar, T. A., and Nam, C., "Aeroservoelastic Tailoring for Lateral Control Enhancement," *Journal of Guidance, Control, and Dynamics*, Vol. 13, No. 3, 1990, pp. 458–465.

A. D. Belegundu
Associate Editor